Lung-selective mRNA delivery of synthetic lipid nanoparticles for the treatment of pulmonary lymphangioleiomyomatosis

Min Qiu[a,1,2], Yan Tang[b,2,3], Jinjin Chen[a,2], Rachel Muriph[c], Zhongfeng Ye[a], Changfeng Huang[a], Jason Evans[c], Elizabeth P. Henske[b,3], and Qiaobing Xu[a,3]

[a]Department of Biomedical Engineering, Tufts University, Medford, MA 02155; [b]Division of Pulmonary and Critical Care Medicine, Brigham and Women's Hospital and Harvard Medical School, Boston, MA 02115; and [c]Department of Chemistry, University of Massachusetts Boston, Boston, MA 02125

Edited by Hongjie Dai, Chemistry, Stanford University, Stanford, CA; received September 2, 2021; accepted January 18, 2022

Safe and efficacious systemic delivery of messenger RNA (mRNA) to specific organs and cells in vivo remains the major challenge in the development of mRNA-based therapeutics. Targeting of systemically administered lipid nanoparticles (LNPs) coformulated with mRNA has largely been confined to the liver and spleen. Using a library screening approach, we identified that N-series LNPs (containing an amide bond in the tail) are capable of selectively delivering mRNA to the mouse lung, in contrast to our previous discovery that O-series LNPs (containing an ester bond in the tail) that tend to deliver mRNA to the liver. We analyzed the protein corona on the liver- and lung-targeted LNPs using liquid chromatography–mass spectrometry and identified a group of unique plasma proteins specifically absorbed onto the surface that may contribute to the targetability of these LNPs. Different pulmonary cell types can also be targeted by simply tuning the headgroup structure of N-series LNPs. Importantly, we demonstrate here the success of LNP-based RNA therapy in a preclinical model of lymphangioleiomyomatosis (LAM), a destructive lung disease caused by loss-of-function mutations in the *Tsc2* gene. Our lung-targeting LNP exhibited highly efficient delivery of the mouse tuberous sclerosis complex 2 (*Tsc2*) mRNA for the restoration of TSC2 tumor suppressor in tumor and achieved remarkable therapeutic effect in reducing tumor burden. This research establishes mRNA LNPs as a promising therapeutic intervention for the treatment of LAM.

lipid nanoparticles | lung-targeted delivery | lymphangioleiomyomatosis | tuberous sclerosis complex | mRNA

The use of messenger RNA (mRNA) for vaccination (1, 2), protein replacement therapy (3) and cancer immunotherapy (4), and mRNA technology encoding CRISPR/Cas nuclease for genome editing (5) holds the potential to revolutionize the treatment of a wide range of currently untreatable genetic diseases. The US Food and Drug Administration (FDA) recently authorized two mRNA vaccines enabled by nonviral lipid nanoparticles (LNPs) against COVID-19 for emergency use, representing a key milestone in mRNA therapeutics. Aside from COVID-19, other mRNA vaccines against influenza viruses (6), Cytomegalovirus (7), and advanced melanoma (8) have also been developed and are now in human clinical trials. The clinical success of these transformative therapeutics is largely reliant on the development of safe, efficient, and highly selective delivery systems to target mRNA toward specific tissues and cell types (9, 10).

As one of the most advanced nonviral synthetic nanoparticles, LNPs have been proven to specifically deliver small interfering RNA (siRNA) to the liver for the treatment of hereditary transthyretin amyloidosis (11). Since mRNA predominantly accumulates in the liver and spleen following systemic delivery (12–16), much of the clinical interest to date has focused on hepatic diseases. Delivery vehicles that enable specific mRNA delivery to extrahepatic tissues are urgently needed to fully realize the potential of mRNA-based therapy. Considerable effort has been made to develop organ-targeted LNPs to bypass liver accumulation by modifying the surface of LNPs with targeting moieties such as peptides, antibodies, and proteins (17–19). Recently, targeted LNPs functionalized with alpha plasmalemma vesicle–associated protein antibody were developed for lung-targeted mRNA delivery in vivo (18). More recently, a selective organ targeting (SORT) strategy was developed to engineer LNPs to tune the biodistribution of LNPs; the incorporation of an extra excipient, the SORT molecule, can enable the precise alteration of the in vivo mRNA delivery profile (20). These strategies exhibit advantages in mitigating liver accumulation and delivering mRNA to lungs or spleens. These promising developments motivate us to continue explore innovative ways to deliver mRNA to specific locations.

A major roadblock in the development of targeted LNPs is difficulty predicting the in vivo targeting behavior of newly designed LNPs due to the limited understanding of the nano-bio interactions between nanoparticles (NPs) and biological components. The outer surface of NPs can be rapidly covered

Significance

The current application of messenger RNA (mRNA)-based technology has largely been confined to liver diseases because of the lack of a specific and efficient extrahepatic in vivo systemic mRNA delivery system. Here, we have developed a library of N-series lipid nanoparticles (LNPs) that could specifically regulate the protein composition of protein corona on the surface of LNPs, which allows specific delivery of mRNA to the lung. We further demonstrated that our lung-targeting LNP could effectively deliver mouse tuberous sclerosis complex 2 (*Tsc2*) mRNA into TSC2-null cells and restore its function, resulting in enhanced control of tumor burden in a preclinical model of lymphangioleiomyomatosis, a destructive lung disease caused by loss-of-function mutations in the *Tsc2* gene.

Author contributions: M.Q., Y.T., and Q.X. designed research; M.Q., Y.T., J.C., R.M., Z.Y., and C.H. performed research; M.Q., Y.T., J.C., R.M., J.E., E.P.H., and Q.X. analyzed data; and M.Q., Y.T., E.P.H., and Q.X. wrote the paper.

Competing interest statement: Q.X., M.Q., and Y.T. are inventors on a pending patent related to this work jointly filed by Tufts University and Brigham and Women's Hospital and Harvard Medical School.

This article is a PNAS Direct Submission.

[1]Present address: Human Phenome Institute, Fudan University, Shanghai 201203, China.

[2]M.Q., Y.T., and J.C. contributed equally to this work.

[3]To whom correspondence may be addressed. Email: Qiaobing.Xu@tufts.edu, ytang11@bwh.harvard.edu, or ehenske@bwh.harvard.edu.

This article contains supporting information online at http://www.pnas.org/lookup/suppl/doi:10.1073/pnas.2116271119/-/DCSupplemental.

Published February 16, 2022.

with a layer of serum proteins, referred to as the "protein corona," which remodels the surface property of NPs and substantially affects the interaction of NPs with organs and cells (21). We and others have demonstrated that the lipidoid amine head structure can impact the delivery efficacy and even the in vivo targetability of mRNA-loaded LNPs (22–24). In a recent study, we showed that imidazole-based synthetic lipidoids preferentially target mRNA to the spleen (25). For the lipidoid tail chemistry, although considerable progress has been made in the understanding of lipidoid tail length, degree of unsaturation, and degree of branching on the effect of mRNA delivery potency (26–29), the influence of lipidoid tail structures on the in vivo selectivity of LNPs remains poorly understood. To address this important knowledge gap, we synthesized a library of amide bond–containing lipidoids (N-series LNPs) via Michael addition reaction between amine heads and acrylamide tails (Fig. 1*A*). Surprisingly, from in vivo screening, we found that the N-series LNPs almost exclusively deliver mRNA to the lung following systemic administration (Fig. 1 *B* and *C*). Intriguingly, our previous study demonstrated that the O-series lipidoids, which contain an ester bond in the tails, tend to deliver mRNA into the liver (16). To better understand why such a small change induces such striking organ specificity, we further investigated the underlying mechanisms of these delivery differences. We hypothesized that once injected into the bloodstream, the LNPs can selectively govern the adsorption of specific plasma proteins to serve as targeting ligands that direct LNPs to selected organs. Indeed, using proteomics, we identified a group of unique plasma proteins specifically absorbed on the surface of two representative LNP candidates, 306-O12B and 306-N16B, that may affect the targetability of these LNPs. More importantly, we found that different pulmonary subcellular populations can be targeted by changing the lipidoid head structure of N-series LNPs. Furthermore, we evaluated the lung-targeting LNPs for the in vivo targeted delivery of *Tsc2* mRNA to TSC2-deficient cells to restore the expression of the TSC2 tumor suppressor for the treatment of pulmonary lymphangioleiomyomatosis (LAM), a rare genetic disorder caused by biallelic mutations and loss of function of TSC complex genes. This study provides proof of concept that tuning the in vivo organ-targeting behavior of LNPs can be achieved by tailoring the composition of protein corona via simple chemistry. This work provides a strategy for the rational design of highly specific organ- and cell-selective LNPs for mRNA-based therapy.

Results

Synthesis of N-Series Lipidoids and In Vivo Screening of mRNA-Loaded LNPs. We generated nine bioreducible N-series lipidoids by reacting the acrylamide tails (N16B, N14B, and N12B) with different commercially available amine heads using a solvent-free Michael addition reaction (Fig. 1*A*). LNPs were then formulated with the previously optimized formulation condition of LNP for mRNA delivery with 50% synthetic active lipidoid, 38.5% cholesterol, 10% 1,2-dioleoyl-sn-glycero-3-phosphocholine (DOPC), and 1.5% 1,2-dimyristoyl-rac-glycero-3-methoxypolyethylene glycol-2000 (DMG-PEG2000) in molar ratios (16). To investigate the in vivo systemic mRNA delivery profiles of these LNPs, we encapsulated firefly luciferase mRNA (fLuc mRNA) encoding firefly luciferase, a reporter protein that can be visualized in vivo using the IVIS imaging system (Perkin-Elmer). Interestingly, the bioluminescence signals in the

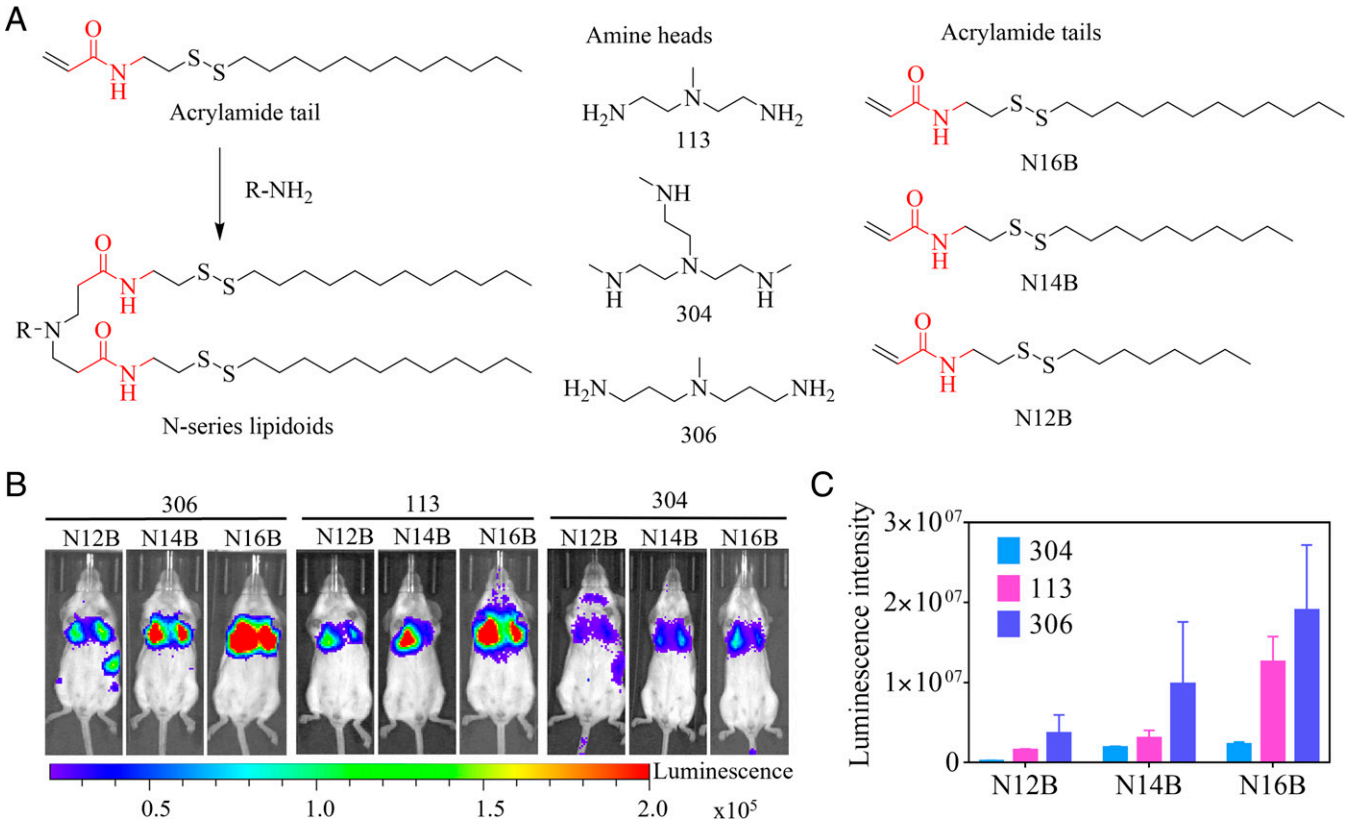

Fig. 1. Synthesis and in vivo screening of N-series LNPs. (*A*) Synthetic route and representative chemical structure of lipidoids. Representative whole-body bioluminescence images of mice (*B*) and in vivo mRNA delivery efficacy (*C*) of N-series LNPs measured by the IVIS imaging system. Mice were injected with either of the Luc mRNA–loaded N-series LNPs at a single dose of 0.5 mg/kg. Images were taken at 6 h postinjection (n = 3). Data are presented as mean ± SD; the error bar around each data point is the SEM.

N-series LNP–treated mice were mainly located in the lungs (Fig. 1*B*). In addition, we found that the chemical structure of lipidoids plays a critical role in determining the in vivo mRNA delivery efficacy of the formulated LNPs. As shown in Fig. 1*C*, the quantified luciferase bioluminescence intensity in the lungs at 6 h postinjection demonstrates that LNPs incorporated with the 306-amine head exhibited the highest delivery efficacy, as compared with the 304 and 113 LNPs. The delivery efficacy also increases with the increasing of the tail length of lipidoids; lipidoids armed with the N16B tail exhibited the highest potency compared with those with an N14B or N12B tail. To investigate whether a helper lipid such as DOPC plays a role in the lung-targeted delivery of these N-series lipidoids, we formulated the 306-N16B with helper lipids such as 1,2-distearoyl-sn-glycero-3-phosphocholine (DSPC) and 1,2-dioleoyl-sn-glycero-3-phosphoethanolamine (DOPE) while keeping cholesterol and DMG-PEG2000 not changed. As shown in *SI Appendix*, Fig. S1, LNP formulation using ionizable lipid 306-N16B with helper lipid DOPE or DSPC also led to the protein expression mainly in the lung, though having less protein production when using helper lipid DOPC (Fig. 1*B*). These results showed that the active lipidoid (e.g., 306-N16B), not the helper lipid, is responsible for the lung-targeted delivery using the N-series LNPs. We then studied the biodistribution of the 306-N16B LNP–mRNA complex to understand the observed organ-selective protein expression. Luc mRNA–loaded LNPs were injected into the Balb/c mice via tail vein injection. Mice were killed and the organs harvested at 4 h postinjection. Then, 306-N16B in the organ was extracted and quantified using mass spectrometry. We found that 306-N16B was not only detected in the lung but also in the liver and some in the spleen (*SI Appendix*, Fig. S2), while luciferase expression was only observed in lung (Fig. 1*B*). Though the specific mechanism for why there is no detectable protein expression in liver and spleen remains to be elucidated, these results showed that there is not always a correlation between LNP organ accumulation and cellular uptake and protein expression.

Different Pulmonary Subcellular Populations Can Be Targeted by Changing the Amine Head Structure of N-Series LNPs. The clinical translation of mRNA-based therapeutics requires specific mRNA delivery to the organs and cell types of interest. The lungs can be affected by many diseases caused by the dysfunction of multiple cellular compartments, including endothelial (30), epithelial (31), and immune cells (32). To identify the lung cell subpopulations that are specifically transfected, we utilized the genetically engineered Cre/LoxP Ai14 reporter mouse line to achieve cell-type–specific expression of the tdTomato protein (33). We injected the Ai14 mice with the two most potent lung-targeting LNPs (306-N16B and 113-N16B). Cre mRNA, encoding Cre recombinase, was used as an mRNA cargo in these experiments. Once delivered into the cells, Cre recombinase removes the stop cassette and activates the expression of tdTomato fluorescence signal in the edited cells (Fig. 2*A*). As shown in the ex vivo image of organs collected from the treated mice (Fig. 2 *B* and *C*), the red tdTomato signal was detected specifically in the lungs of both 306 and 113-N16B LNP–treated mice, and tdTomato positive cells were observed by using confocal imaging of lung sections. To further identify and quantify the transfected specific cell types in the lungs, lung tissues were processed into single-cell suspensions and analyzed using flow cytometry. For the 306-N16B LNP, 33.6% of pulmonary endothelium was transfected, compared with 1.5% of epithelium and 1.9% of macrophages (Fig. 2*B*), indicating that the 306-

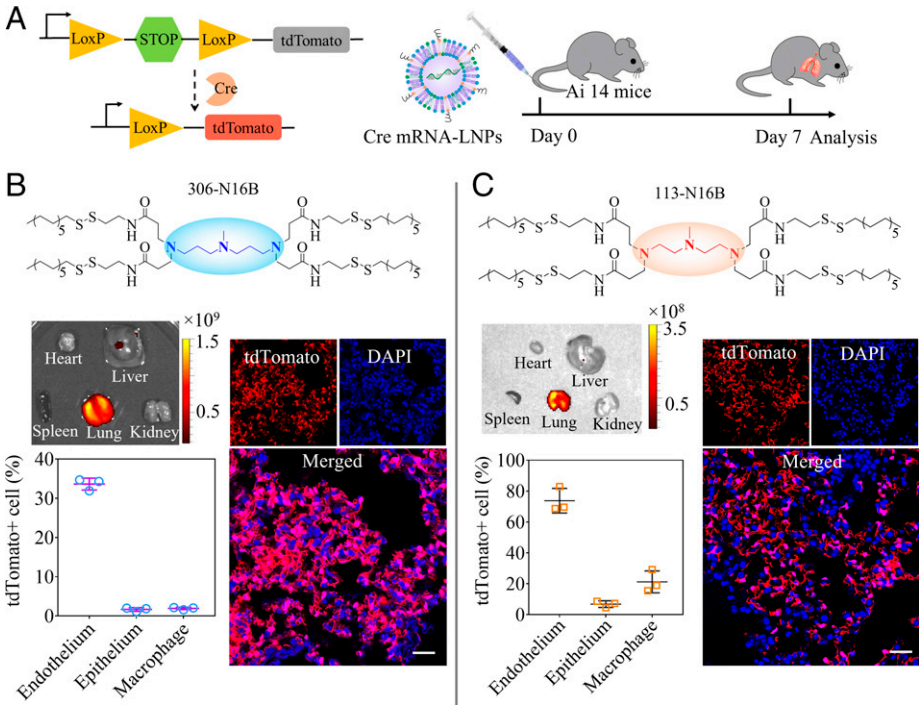

Fig. 2. Different pulmonary cell types can be targeted by tuning the head structure of N-series LNPs. (*A*) Schematic illustration of the delivery of Cre mRNA to the lung to activate tdTomato expression via Cre-mediated genetic deletion of the stop cassette in tdTomato transgenic Ai14 mice. (*B, C*) Chemical structure, representative ex vivo image of tdTomato fluorescence in edited Ai14 mouse organs captured by using the IVIS imaging system, representative immunofluorescence images of lung tissue taken by confocal microscopy, and quantification of the percentage of tdTomato+ cells within defined cell types of the lungs by flow cytometry of 306-N16B (*B*) and 113-N16B (*C*) LNPs. Mice were i.v. injected with Cre mRNA–loaded LNPs at a single dose of 0.75 mg mRNA equiv./kg. Endothelial cells were stained by FITC (fluorescein isothiocyanate)-CD31 antibody, epithelial cells were stained by CD326-PE-Cy7 antibody, and macrophages were stained by F4/80-eFluor 660 antibody (Scale bar, 20 μm).

N16B LNP is capable of selectively delivering mRNA to the pulmonary endothelial cells. In contrast, the 113-N16B LNP delivered Cre mRNA preferentially to endothelial cells (69.6% of total endothelial cells were transfected) but also to macrophages (18.9%) and epithelium (7.3%) (Fig. 2*C*). These findings demonstrate that different pulmonary cell populations can be targeted by simply tuning the head structure of N-series LNPs, setting the stage for potential therapeutic applications for lung diseases associated with specific pulmonary cells.

Characterization of Proteins Constituting the Protein Corona in 306-O12B LNP and 306-N16B LNP. It is believed that the outer surface of nanoparticles (NPs) is immediately masked with a layer of biomolecular corona shortly after intravenous administration, which can dramatically alter the surface properties of NPs and determine their in vivo fate (34). The controlled adsorption of specific plasma proteins on the NPs surface may selectively direct NPs to specific organs (35–37). We previously reported that O-series LNPs could specifically deliver mRNA to the liver (16). We hypothesized that the dramatically different in vivo organ targetability of O- and N-series LNPs (Fig. 3*A*) might be attributed to the serum proteins formed on their surfaces (Fig. 3*B*). To test this hypothesis, we identified and quantified the proteins on two representative LNPs, 306-O12B and 306-N16B. We incubated these two LNPs with mouse plasma at 37 °C for 1 h and isolated and recovered the protein-coated LNPs using centrifugation followed by extensive washing with PBS. Proteomics was then performed to analyze the composition of proteins on LNPs. We identified and quantified 1,838 and 1,088 proteins on the 306-O12B LNP and 306-N16B LNP, respectively. The complete dataset containing the molecular mass and calculated isoelectric point of all identified proteins is provided in Dataset S1. Venn diagrams revealed both common and unique proteins between the 306-O12B LNP and the 306-N16B LNP (*SI Appendix*, Fig. S3). We listed the top 20 most abundant corona proteins, which may play the dominant role in the protein corona, for each LNP in Table 1. We found that 306-O12B LNP and 306-N16B LNP only shared six common proteins among the top 20, supporting our hypothesis that the proteins absorbed on the LNP surface may participate in the in vivo targetability. We identified ApoE as the second dominant protein composition in the corona of the liver-targeting 306-O12B LNP (Fig. 3*C*), consistent with a prior study demonstrating apolipoprotein E (ApoE)–mediated delivery of LNPs to the liver (11). In contrast, the top three proteins in the corona of the lung-targeting 306-N16B LNP are serum albumin, fibrinogen beta chain, and fibrinogen gamma chain (Fig. 3*D*). It has been reported that fibrinogen coating can improve endothelial cell adhesion and endothelialization (38, 39). Dissecting whether the underlying mechanisms of protein corona–mediated liver- or lung-targeted mRNA delivery by O-series or N-series LNPs, respectively, are determined by one particular protein or the synergistic effects of several proteins needs further study.

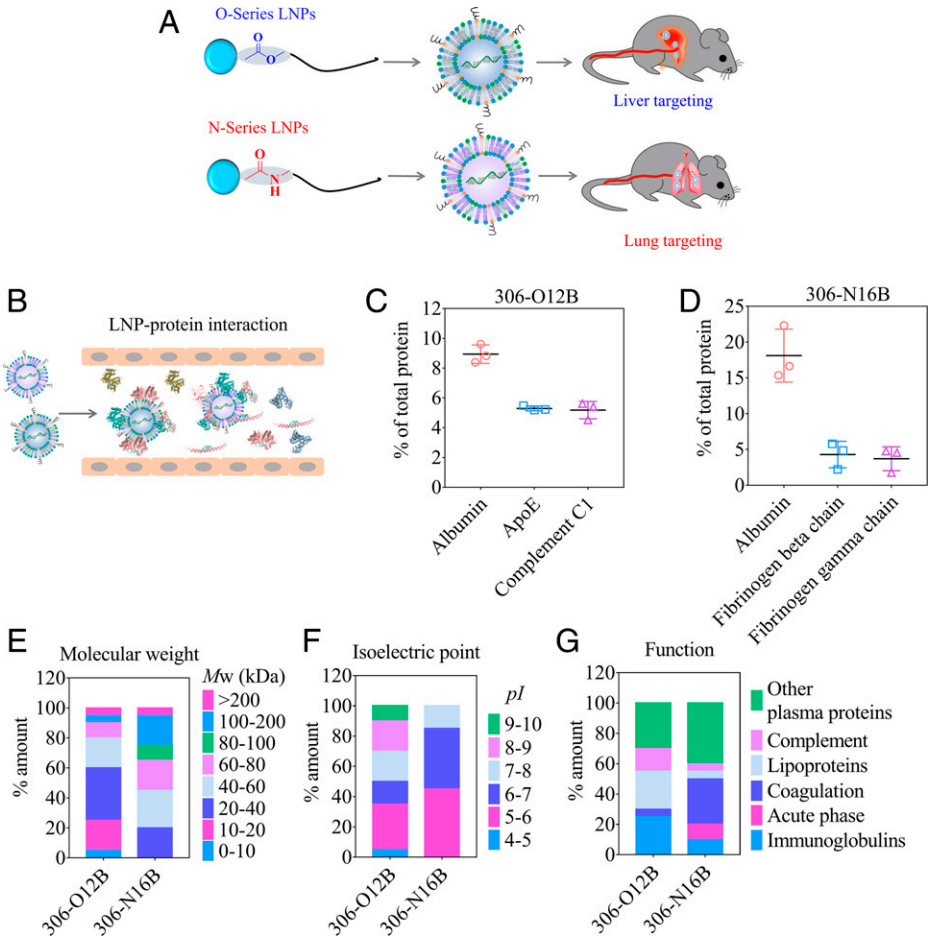

Fig. 3. Proteomics study of protein coronas formed on LNPs. (*A*) Schematic illustration of different organ targetability of O- and N-series LNPs. (*B*) Interaction of LNPs with proteins in the blood vessel. Quantification of percentage of total proteins of the top three protein components in the protein corona of the 306-O12B LNP (*C*) and the 306-N16B LNP (*D*) is shown ($n = 3$). The top 20 most abundant corona proteins were categorized based on their calculated molecular weight (*E*), isoelectric point (*F*), and biological function (*G*).

Table 1. Top 20 most abundant corona proteins identified in the protein corona of LNPs

No.	306-O12B	306-N16B
1	albumin	albumin
2	**apolipoprotein E**	fibrinogen beta chain
3	**complement C1q subcomponent subunit B**	**fibrinogen gamma chain**
4	immunoglobulin heavy constant mu	**fibrinogen alpha chain**
5	apolipoprotein A-I	**fibronectin**
6	**complement C1q subcomponent subunit C**	**ceruloplasmin**
7	**complement C1q subcomponent subunit A**	immunoglobulin heavy constant alpha (fragment)
8	**apolipoprotein B-100**	**prothrombin**
9	**beta-globin**	immunoglobulin heavy constant mu
10	**apolipoprotein A-IV**	**complement C3**
11	**apolipoprotein C-I**	**H-2 class I histocompatibility antigen, Q10 alpha chain**
12	**serotransferrin**	**interalpha-trypsin inhibitor heavy chain H3**
13	**pregnancy zone protein**	**carboxylesterase 1C**
14	immunoglobulin heavy constant alpha (fragment)	apolipoprotein A-I
15	**immunoglobulin kappa constant**	vitronectin
16	**immunoglobulin kappa variable 17–121 (fragment)**	**interalpha-trypsin inhibitor heavy chain H2**
17	fibrinogen beta chain	**protein AMBP**
18	**alpha globin 1**	**interalpha-trypsin inhibitor heavy chain H1**
19	**immunoglobulin heavy constant gamma 2C (fragment)**	**alpha-1-antitrypsin 1–4**
20	vitronectin	**bradykinin**

Proteins in bold text are unique proteins among the top 20 for indicated LNPs.

We further classified the top 20 proteins according to their molecular weight (Mw) (Fig. 3*E*). The protein corona of the 306-O12B LNP was enriched in low molecular weight proteins with 80% of proteins having an Mw < 60 kDa, while 55% of proteins in the protein corona of the 306-N16B LNP are larger than 60 kDa. We also categorized the proteins based on their isoelectric point (pI). As shown in Fig. 3*F*, 50% and 80% of proteins displaying a negative charge (pI < 7) at physiological pH 7.4 constitute the protein corona of the 306-O12B LNP and 306-N16B LNP, respectively. It was suggested that positively charged NPs prefer to attract negatively charged proteins (40). However, in our case, we did not see a significant difference in the zeta potential of these two LNPs, with both LNPs showing a slight negative surface charge (*SI Appendix*, Table S1), indicating that surface charge may not be the only factor that affects the interaction between NPs and proteins in the biological fluids. Finally, we sorted the proteins according to their biological functions (Fig. 3*G*). Proteins abundant on the 306-O12B LNP and 306-N16B LNP are associated with lipid metabolism, complement activation, immune responses, acute-phase response, and coagulation. It should be noted, however, that aside from the other plasma proteins, the highest enriched proteins in the corona of the 306-O12B LNP are the apolipoproteins that involve in lipid and cholesterol metabolism (Fig. 3*G*), while coagulation-relevant corona proteins represent the largest fraction in the corona of the 306-N16B LNP (Fig. 3*G*). Collectively, these findings illustrated that the protein coronas formed on the 306-O12B LNP and 306-N16B LNP differ in protein compositions, fractions, and biological functions, which may play critical roles in determining their in vivo tissue targeting.

306-N16B LNP Allows Lung-Specific Delivery of Genome-Editing Cas9 mRNA. As we have demonstrated above, the 306-N16B LNP is capable of specifically delivering fLuc mRNA and Cre mRNA to the lungs. The length of these two mRNAs is less than 2,000 nucleotides (1,960 nucleotides for fLuc mRNA and 1,350 nucleotides for Cre mRNA). Some specific diseases may require the delivery of even larger mRNA molecules. With this in mind, we wondered whether our 306-N16B LNP could similarly have the potential to deliver longer mRNA to the lung. We thus formulated a 306-N16B LNP with Cas9 mRNA, a genome-editing mRNA that has 4,521 nucleotides, which is more than three times longer than the fLuc mRNA; the LNP was then injected into the Babl/c mice. After 6 h, mice were killed, and organs were collected for further Western blot analysis to detect the Cas9 protein expression in different organs. Notably, we found that the Cas9 protein can be only detected in the lung (*SI Appendix*, Fig. S4), indicating that the 306-N16B LNP mediated specific delivery of Cas9 mRNA to the lung.

After confirming that the 306-N16B LNP could specifically deliver Cas9 mRNA to the lungs, we next reasoned whether we can codeliver Cas9 mRNA and a single guide RNA (sgRNA) in the 306-N16B LNP to the lungs to enable lung-specific CRISPR-Cas9 genome editing. To test this hypothesis, we injected Ai14 mice with Cas9 mRNA and a LoxP-targeting sgRNA (sgLoxP)–loaded 306-N16B LNP at a dose of 1.67 mg/kg of total RNA (Cas9 mRNA/sgLoxP = 1:1.2, wt/wt) and analyzed gene editing specificity at day 7 postinjection (Fig. 4*A*). As shown in Fig. 4*B*, fluorescence signals were mainly seen in the lungs; a weak fluorescence signal was also observed in the liver. tdTomato positive cells were seen from the microscopy images of tissue sections (Fig. 4*C*). The results indicated that 306-N16B LNP was able to codeliver Cas9 mRNA and sgRNA to both lungs and liver in mice to allow genome-editing applications. However, we found that the 306-N16B LNP showed less tissue selectivity in codelivering Cas9 mRNA and sgRNA as compared with the single mRNA delivery that could almost exclusively deliver mRNA to the lungs. This indicates that the incorporation of a shorter sgRNA could alter the physical property of formed LNP and change the organ-tropism of LNP. The observation that including additional components into the LNP formulation can change delivery efficiency and tropism was previously reported in the literature (20, 41, 42).

LNP for Lung-Targeted TSC2 mRNA Delivery for the Treatment of LAM In Vivo. Pulmonary LAM is a rare genetic lung disease that is characterized by aberrant mTORC1 hyperactivity caused by inactivating mutations of the tuberous sclerosis complex 1 or 2 (*Tsc1* or *Tsc2*) genes. Rapamycin (sirolimus), an mTORC1 inhibitor, is FDA-approved for the treatment of LAM (43–46), although ongoing loss of lung function and need for lung transplantation can still occur (47). Thus, there is an urgent need to develop new therapies for the treatment of LAM. Therefore,

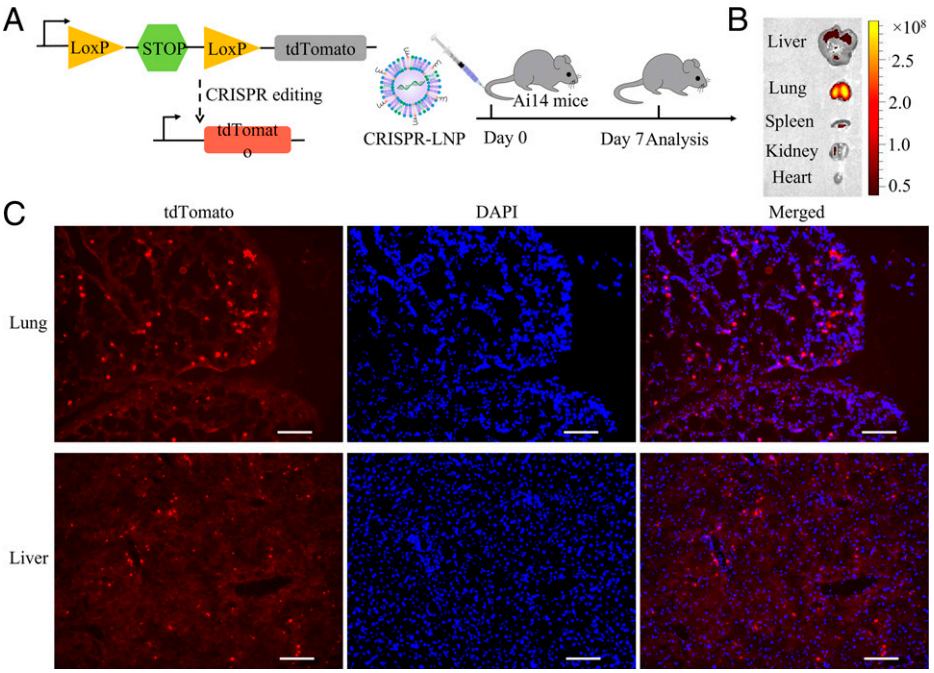

Fig. 4. The 306-N16B LNP allows systemic codelivery of Cas9 mRNA and sgRNA in vivo. (*A*) Schematic illustration of codelivery of Cas9 mRNA and sgLoxP to activate the tdTomato expression in Ai14 mice. (*B*) Representative ex vivo image of organs collected from Cas9 mRNA and sgLoxP coloaded 306-N16B LNP–treated transgenic Ai14 mice. Mice were injected via tail vein at a dosage of 1.67 mg/kg of total RNA. (*C*) Representative microscopy images of the lung and liver dissected from Cas9 mRNA and sgLoxP coencapsulated 306-N16B LNP–treated Ai14 mice (Scale bar, 100 μm).

we evaluated whether our lung-targeting LNPs can deliver mRNA encoding the *Tsc2* gene for the treatment of LAM.

We first tested the feasibility of our LNPs to deliver enhanced green fluorescent protein (EGFP) mRNA into mouse TSC2-null TTJ cells (Tsc2-null, kidney-derived epithelial tumor cells), which are used in an established model of LAM (48). In vitro, we found that the lung-targeting 306-N16B LNP showed low delivery efficacy in transporting mRNA to TTJ cells, but the liver-targeting 306-O12B LNP exhibited a relatively higher transfection efficiency (*SI Appendix*, Fig. S5). Therefore, we designed a hybrid LNP formulated with an equimolar mixture of 306-O12B and 306-N16B (referred to as hLNP) (Fig. 5*A*). We hypothesize that such hLNPs can efficiently target the lungs and also deliver cargo to the TTJ cells in vivo. Interestingly, such hLNPs showed a much higher transfection efficiency toward TTJ cells when compared with the 306-O12B and 306-N16B LNPs, and uniform expression of EGFP was observed (*SI Appendix*, Fig. S5). An in vivo imaging study also revealed that the hLNP delivers Luc mRNA to both the lung and liver (*SI Appendix*, Fig. S6). In the application to replace a mutated gene for cancer therapy, it may not be a concern of delivering wild-type mRNA to the liver, which naturally expresses TSC2.

To determine whether an hLNP can deliver mRNA to TSC2-deficient cells in vivo, TTJ cells were injected intravenously into syngeneic 6-wk–old C57BL/6J mice to form LAM-like nodules in the lung as previously reported (48). hLNPs encapsulating EGFP mRNA were injected via tail vein. We killed the mice and collected the lungs 6 h after injection. EGFP expression in the lung was analyzed through immunohistochemistry (IHC). Remarkably, as shown in Fig. 5*B*, EGFP expression was primarily detected in TTJ-derived tumor nodules, but not in adjacent normal lung tissue. Phospho-S6 (a marker of TSC2-deficient cells) immunostaining revealed strong colocalization of phospho-S6 and EGFP (Fig. 5*C*), confirming that hLNP enables specific delivery of EGFP mRNA to TTJ cells.

We next evaluated the therapeutic effect of hLNPs loaded with *Tsc2* mRNA in this preclinical model. Full-length (5,445 nucleotides) mouse wild-type *Tsc2* mRNA was transcribed in vitro. In vitro, this mRNA suppressed the expression of phospho-S6 in TSC2-null cells (*SI Appendix*, Fig. S7 *A* and *B*), indicating successful suppression of the mTORC1 pathway. Similarly, re-expressing wild-type *Tsc2* mRNA in patient-derived TSC2-deficient cells significantly inhibited mTORC1 signaling (*SI Appendix*, Fig. S7 *C* and *D*). We treated TTJ tumor-bearing mice with *Tsc2* mRNA–encapsulated hLNP (0.75 mg/kg) or empty hLNP, every other day for a total of five doses, starting on day 24 after TTJ cell inoculation, with five mice in each treatment group. Mice without treatment were also included as a control (Fig. 6*A*). The *Tsc2* mRNA–loaded hLNP significantly suppressed tumor growth compared to that of empty LNPs or without treatment (Fig. 6*B*; *SI Appendix*, Fig. S8). No significant difference was observed between the empty LNP treatment group and the untreated group. We further evaluated tumor proliferation and apoptosis using IHC against Ki67 and cleaved caspase 3, respectively (Fig. 6 *C* and *D*). Cell proliferation within tumor modules was decreased by *Tsc2* mRNA LNP treatment compared to that of empty LNP and untreated groups, while no difference was observed between empty LNP and untreated groups. The difference of tumor cell apoptosis between the empty LNP and untreated groups is very small, indicating that tumor apoptosis may not be a major mechanism of tumor reduction in this model. We hypothesize that wild-type TSC2 restoration through mRNA delivery may thus induce immune-mediated mechanisms that reduce the TTJ cells' tumor burden (49). To test this possibility, we assessed macrophage and T cell tumor infiltration by IHC against F4/80 and CD3. No difference in macrophage infiltration was observed between the groups, but the *Tsc2* mRNA–loaded hLNP treatment group showed enhanced tumor T cell infiltration (Fig. 6*D*), consistent with the hypothesis that restoration of TSC2 protein expression induces an immune-mediated therapeutic response in this preclinical model of LAM.

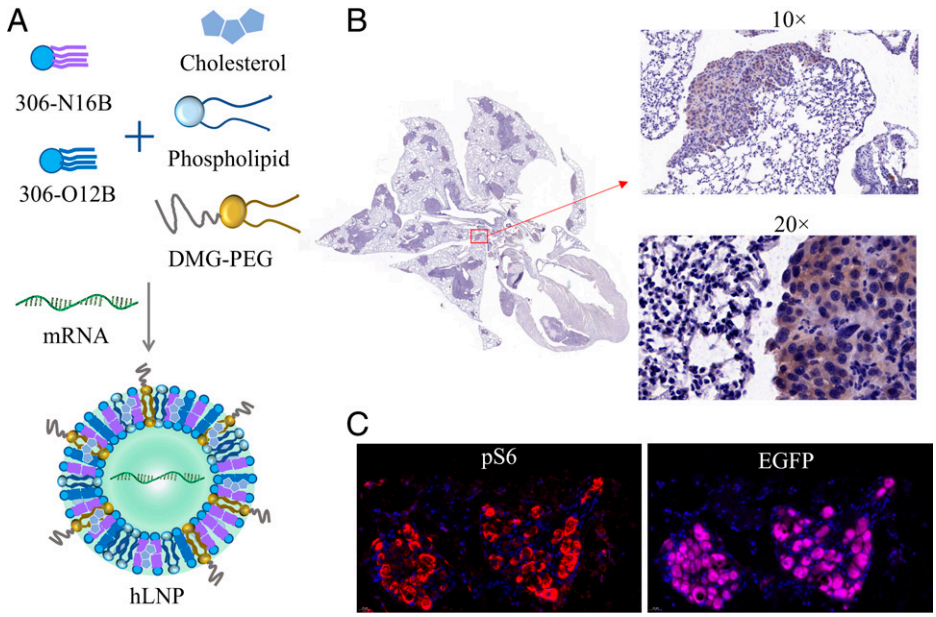

Fig. 5. hLNP enables specific delivery of mRNA to the TTJ tumor cells in vivo. (*A*) Schematic illustration of the preparation of hybrid LNP. hLNP was formulated at a molar ratio of 25:25:38.5:10:1.5 of 306-N16B:306-O12B:cholesterol:DOPC:DMG-PEG2000. (*B*) Representative images of IHC analysis of EGFP in mouse LAM lungs. Syngeneic C57BL/6J mice were tail vein injected with TSC2-deficient TTJ cells to form tumor nodules in the lungs. Mice were tail vein injected with an hLNP loaded with EGFP mRNA. Lungs were collected 6 h postinjection. (*C*) Multiplex immunofluorescence staining shows colocalization of pS6 (a marker of tumor cell) and EGFP. (*Left*) Staining of pS6; (*Right*) staining of EGFP.

Discussion

In recent years, increasing interest has been seen in using the LNPs to deliver mRNA therapeutics. The in vitro synthetic mRNA has the potential to produce therapeutically relevant proteins "in vivo" to control and treat a broad spectrum of diseases, including AIDS, Zika, rare diseases, cancer, and coronavirus. To leverage this transformative technology to benefit human health, the mRNA needs to be sent to the diseased organs and cells to enable specific expression of therapeutic proteins, and subsequently, produce the desired therapeutic effect. LNPs represent one of the leading nonviral delivery systems for nucleic acid delivery, and considerable efforts have been made to employ LNPs for mRNA delivery. However, the fact is that the majority of developed LNPs have targeted the liver after systemic administration; therefore, new strategies are needed to direct LNPs to other organs, such as the lungs, kidneys, heart, and brain. Currently, we and others have reported that some LNPs containing specific amine heads, such as imidazole, adamantly, and neuron transmitter, delivered mRNA, siRNA, and antisense oligonucleotide (ASO) to the spleen and brain (22, 25, 50). More recently, the Siegwart laboratory discovered and developed an SORT strategy to engineer LNPs to target extrahepatic tissues, for example, the lung and spleen, with the addition of an extra excipient (20).

Here, we show that the in vivo organ selectivity of LNPs can be precisely tuned by simply changing the linker structure in the lipidoid tails without complicating the LNP formulation. By changing the linker from ester bond (referred to as O-series) to amide bond (referred to as N-series), the mRNA delivery specificity enabled by LNPs was switched from the liver to the lung. A proteomic study was performed to try to explain why such a small structural difference between the O-series and N-series LNPs leads to dramatically different organ selectivity. The primary hypothesis is that these two tail structures may have a specific affinity to some distinct serum proteins that dictate the protein compositions of coronas formed on the surface of the LNPs during the circulation. It has been reported that the protein corona plays a key role in determining the in vivo fate of nanoparticles. Our results showed that the number and type of plasma proteins in the protein coronas of 306-O12B and 306-N16 LNPs are different. We found 14 distinct proteins among the top 20 most abundant proteins in these two LNPs, which may contribute to the organ-selective protein expression.

Targeted RNA delivery to the lung is an attractive concept, which offers tremendous opportunities to explore targets that are currently be defined as "undruggable" for the treatment of a broad spectrum of pulmonary diseases. In this study, we demonstrated that different pulmonary cells can be easily targeted by tuning the head structure of LNPs. We showed that the 306-N16B LNP can specifically transport mRNA to the pulmonary endothelial cells, an important therapeutic target that involves acute respiratory distress syndrome, inflammation, and thrombosis (30). However, mRNA containing the 113-N16B LNP was able to transfect not only pulmonary endothelial cells but also macrophages and even epithelial cells after systemic administration. Furthermore, we also demonstrated that codelivering Cas9 mRNA and sgRNA into one single 306-N16B LNP achieved genome editing in the lungs of mice, which may allow further development of genome editing–based therapies for the treatment of pulmonary genetic diseases. More importantly, we demonstrated that our developed hybrid LNP was able to specifically deliver *Tsc2* mRNA to TSC2-deficient TTJ tumor cells in a preclinical LAM model and significantly inhibit tumor cell growth, providing critical proof of concept for the use of LNP for the treatment of pulmonary diseases.

In summary, this study demonstrated a strong correlation of the structure-activity relationships between lipidoid tail chemistry and organ and cell selectivity for mRNA delivery. The mechanistic study using proteomics indicated that the protein composition in the protein coronas of these two LNPs are different, suggesting the unique tail linker structures may have a profound impact on the interaction of LNPs and biological fluids that substantially influence the targetability of LNPs. However, further studies should be performed to fully elucidate the effect of these unique proteins on organ targetability. The findings from this work provide a fundamental understanding of how lipid structure may

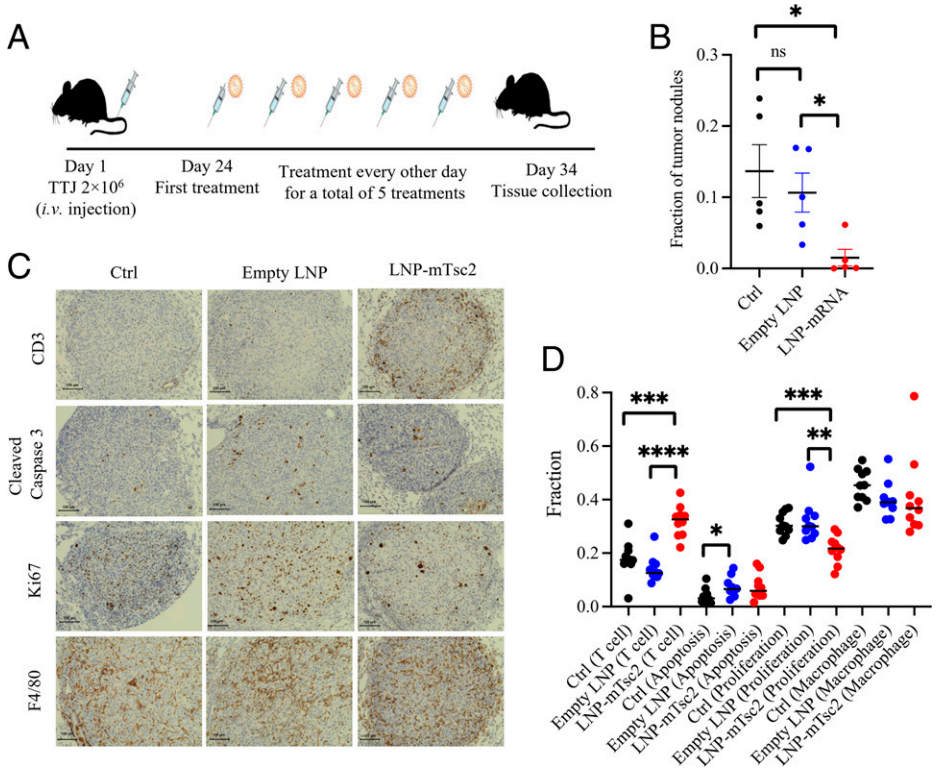

Fig. 6. Therapeutic effect of TSC2 mRNA–loaded hLNP in antitumor growth. (*A*) Treatment design. Syngeneic C57BL/6J mice were tail vein injected with 2×10^6 TSC2-deficient TTJ cells to form tumor nodules in the lung. On day 24 after tumor cell inoculation, mice were randomly assigned to three groups: untreated control, empty LNP treatment, and LNP-mTsc2 (0.75 mg/kg of mRNA per injection) treatment. Mice were treated every other day for a total of five times ($n = 5$). (*B*) Fraction of tumor nodules per lung in the three treatment groups. (*C*) Representative images of IHC assessment of ki67, cleaved caspase 3, macrophages, and CD3 in empty hLNP and TSC2 mRNA–loaded hLNP. (*D*) Quantitative analysis of *C*. Ten images were analyzed for each group. T cell: CD3 IHC; apoptosis: cleaved caspase 3 IHC; proliferation: Ki67 IHC; macrophage: F4/80 IHC. Data are shown in mean ± SD; the error bar around each data point is the SEM. Student's *t* test was used to calculate the statistical significance. $*P < 0.05$, $**P < 0.01$, $***P < 0.001$, $****P < 0.0001$.

affect the in vivo fate of LNPs by manipulating protein corona functions. We believe this study will provide insights into the rational and predictable design of organ-targeted LNPs via simple chemistry for the development of mRNA-based therapy.

Materials and Methods

Lipidoid Nanoparticle Synthesis. Lipidoids were synthesized through the Michael addition reaction between amine heads and alkyl-acrylate tails as in previous reports (51, 52). Lipidoid nanoparticles were formulated by rapidly mixing active lipidoids, cholesterol (Sigma-Aldrich), DOPC or DOPE or DSPC (Avanti Polar Lipids), and $mPEG_{2000}$-DMG (Avanti Polar Lipids) at a molar ratio of 50:38.5:10:1.5 in ethanol solution with sodium acetate buffer (pH 5.2, 25 mM) containing mRNA by using the NanoAssemblr microfluidic system. The final weight ratio of active lipidoid to mRNA was set at 10/1. The resulting LNPs were further dialyzed against phosphate buffered saline (PBS) (10 mM, pH 7.4) in 3,500 MWCO (molecular weight cut off) cassettes (Thermo Fisher Scientific) overnight at 4 °C. The size and surface zeta potential of LNPs were measured by using a ZetaPALS DLS machine (Brookhaven Instruments).

In Vivo mRNA Delivery. All animal experiments were conducted in accordance with the approved animal protocols. For in vivo fLuc mRNA transfection, female Balb/c mice aged 6 to 8 wk purchased from Charles River were intravenously (i.v.) administered with fLuc mRNA–loaded LNPs (0.5 mg/kg mRNA). At 6 h postinjection, mice were intraperitoneally injected with D-Luciferin (Goldbio, 15 mg/mL in PBS) and imaged by using the IVIS imaging system (PerkinElmer). To further quantify the luciferase protein expression in different organs, tissues were harvested, homogenized, and centrifuged to collect the supernatant. The supernatant was then assayed for luciferase expression using Firefly Luciferase Assay Kit 2.0 (Biotium). The results were presented as nanogram luciferase protein per gram of tissue.

For gene-recombinant Cre mRNA delivery, LNPs coformulated with Cre mRNA were i.v. injected into Ai14 Cre reporter mice (The Jackson Laboratory). After 7 d, mice were killed, and major organs were collected and imaged using an IVIS imaging system. To further identify the specific cell populations that were transfected, tissues were frozen, sectioned into 10 μm in depth, and further imaged by using an SP8 confocal microscope (Leica). For flow cytometry studies, lungs were minced and then treated with a mouse Lung Dissociation Kit (Milteny Biotec). Next, the lung solution was filtered through a 70-μm strainer to proceed to single-cell suspension, centrifuged, and then treated with red blood cell lysis buffer (eBioscience) for 5 min. The solution was then centrifuged again to harvest a cell pellet. Cells were resuspended in flow cytometry staining buffer (eBioscience), and then antibodies were added and incubated for 30 min on ice in the dark. The stained cells were washed twice with cold PBS, resuspended in PBS, and measured using an LSR-II flow cytometer (BD Bioscience). The antibodies used in this study are as follows: CD326-PE-Cy7 (eBioscience), CD31-FITC (Biolegend), and F4/80-eFluor 660 (eBioscience). The dilution rates of all antibodies were used as per manufacturers' suggestions.

For genome-editing Cas9 mRNA delivery, Cas9 mRNA–loaded LNPs were i.v. injected into Balb/c mice (0.5 mg/kg); 6 h postinjection, mice were killed, organs were collected, and Western blot was performed to detect the Cas9 expression in different organs. Briefly, organs were homogenized in lysis buffer and centrifuged at 13,000 × *g* for 10 min at 4 °C. The supernatants were collected, and the protein concentrations were measured using a BCA (bicinchoninic acid) assay kit (Thermo Fisher Scientific). Then, 20 μg of total proteins was loaded onto a 4 to 20% polyacrylamide gel (Thermo Fisher Scientific), and the gel was then run for 90 min under a stable voltage of 120 V. The gel was cut and transferred to a polyvinylidene difluoride (PVDF) membrane, blocked with 5% skimmed milk for 1 h at room temperature, and incubated with anti–CRISPR-Cas9 primary antibody (Abcam, ab189380) overnight at 4 °C. The membrane was washed with TBST (Tris-buffered saline, 0.1% Tween 20) five times, incubated with horseradish peroxidase (HRP) rabbit anti-mouse secondary antibody (Abcam) for 1 h at room temperature, and then imaged with an enhanced chemiluminescence (ECL) substrate using a gel imaging system.

In Vivo Biodistribution of LNPs. The Luc mRNA–encapsulated 306-N16B LNP was injected into the Balb/c mice through i.v. injection at an mRNA dosage of 0.5 mg/kg. Mice were killed at 4 h postadministration, and main organs (heart,

liver, lung, spleen, and kidney) were collected. An ~50-μg aliquot of tissue samples was used for lipid extraction. Briefly, tissue sample was placed in a 1.5-mL EP tube, and 1 mL of methanol was added and dissociated by Beadbud machine to extract lipids. The extracted lipid samples were measured using mass spectrometry after filtration. A standard curve was used to correlate the area under the curve of the extracted ion chromatograms to a quantitative amount of lipid.

Isolation of Protein Corona. Mouse plasma was centrifugated at 13,000 × *g* at 4 °C to remove protein aggregates before use. LNPs were mixed with an equal volume of C57BL/6 mouse plasma to mimic the protein concentration in vivo and incubated for 1 h at 37 °C under shaking (40). The protein corona–coated LNPs were isolated by centrifugation at 13,000 × *g* for 30 min, followed by washing with cold PBS three times to remove unbound proteins. The same procedure was performed for plasma aliquots without adding the LNPs to verify the absence of protein precipitation. All experiments were conducted three times. The amount of protein in protein corona–coated LNPs was determined using a BCA assay kit (Thermo Fisher Scientific). The obtained protein samples were further lyophilized and stored at −20 °C for further experiment.

Reduction, Alkylation, and Digestion of Proteins. The lyophilized protein samples were reconstituted to 1 mg/mL in M-PER Mammalian Protein Extraction Reagent (Thermo Fisher Scientific). For each sample, 100 μg of protein was reduced with 2.1 μL of 500 mM dithioerythritol, 99+% (Acros Organics) at 50 °C for 45 min. The samples were then alkylated with 11.5 μL of iodoacetamide (Acros Organics) in the dark for 30 min at room temperature. The samples were then digested with trypsin/Lys-C Mix (Mass Spec Grade, Promega) overnight at 37 °C at an enzyme/protein ratio of 1:50. The samples were then stored at −20 °C until liquid chromatography–mass spectrometry analysis.

Mass Spectrometry. The resulting samples were further analyzed by electrospray liquid chromatography–tandem mass spectrometry using an Orbitrap Fusion Lumos mass spectrometer (Thermo Fisher Scientific) coupled online to an EASY-nLC 1200 (Thermo Fisher Scientific). Samples were run at a flow rate of 300 nL/min using the following gradient: 0 to 4 min 0 to 5% B, 4 to 74 min 0 to 30% B, 74 to 79 min 30 to 90% B, 79 to 89 min 90% B, 89 to 94 min at 90 to 0% B, and 94 to 105 min 0% B for column re-equilibration. Mobile phase A was 96.1:3.9 0.1% formic acid (FA) in water/0.1% FA in acetonitrile (ACN). Mobile phase B was 80.0:20.0 0.1% FA in water/0.1% FA in ACN. The samples were first desalted on a Thermo Fisher Scientific Acclaim PepMap 100 C18 HPLC column (3 μm particle size, 75 μm × 2 cm, 100 Å) before separation on a Thermo Fisher Scientific PepMap RSLC C18 EASY-Spray Column (3 μm particle size, 75 μm × 15 cm, 100 Å). The data were analyzed using the Proteome Discoverer 2.1.0.81 software (Thermo Fisher Scientific). The data were run against the *Mus musculus* Uniprot FASTA file (modified 26 August 2020) to identify the mouse proteins in the corona.

In Vitro mRNA Delivery. The TSC2-deficient TTJ cells were seeded in 48-well plates with 1×10^4 cells per well. After 24-h incubation, cells were transfected with EGFP mRNA by using LNPs (100 ng of mRNA per well) for 24 h. Lipofectamine2k was used as a positive control. To measure the transfection efficiency, cells were digested with trypsin, collected, and further evaluated the GFP expression using flow cytometry (Attune NxT Cytometer; Thermo Fisher Scientific). The percentage of EGFP-positive cells was calculated by Flowjo.

In Vitro Transcription of *TSC2*/*Tsc2* mRNA. Full-length human *TSC2* or mouse *Tsc2* gene was cloned into In Vitro Transcription Vector for mRNA (VectorBuilder) driven by T7 promotor. Human *TSC2* gene has an internal T7 terminator, which was corrected by a synonymous mutation (G264C). Vectors were digested using restriction endonuclease AscI (NEB, catalog no. R0558) according to manufacturer's protocol. Capped RNA was synthesized using mMESSAGE mMACHINE T7 Transcription Kit (Thermo Fisher Scientific, catalog no. AM1344) according to the manufacturer's protocol. Synthesized RNA was purified by LiCl precipitation. RNA quality was assessed by Bioanalyzer.

In Vivo Treatment of TTJ Tumor with *Tsc2* mRNA. C57BL/6 mice were tail vein injected with 2×10^6 TSC2-deficient TTJ cells to form tumor nodules in the lungs. On day 24 after tumor cell inoculation, mice were randomly assigned to three groups: untreated control group, empty LNP treatment group, and *Tsc2* mRNA–loaded LNP (dosage: 0.75 mg/kg of mRNA per injection) treatment group. Mice were treated every other day for a total of five times. After treatment, mice were killed, and lungs were collected for further morphological and immunohistochemical analyses.

Data Availability. All study data are included in the article and/or *SI Appendix*.

ACKNOWLEDGMENTS. Q.X. acknowledges support by NIH Grant No. UG3 TR002636-01. Y.T. acknowledges financial support by the LAM Foundation career development Grant No. LAM0142C01-20.

1. N. Pardi, M. J. Hogan, F. W. Porter, D. Weissman, mRNA vaccines—A new era in vaccinology. *Nat. Rev. Drug Discov.* **17**, 261–279 (2018).
2. G. Maruggi, C. Zhang, J. Li, J. B. Ulmer, D. Yu, mRNA as a transformative technology for vaccine development to control infectious diseases. *Mol. Ther.* **27**, 757–772 (2019).
3. U. Sahin, K. Karikó, Ö. Türeci, mRNA-based therapeutics—Developing a new class of drugs. *Nat. Rev. Drug Discov.* **13**, 759–780 (2014).
4. F. Pastor *et al.*, An RNA toolbox for cancer immunotherapy. *Nat. Rev. Drug Discov.* **17**, 751–767 (2018).
5. H. X. Zhang, Y. Zhang, H. Yin, Genome editing with mRNA encoding ZFN, TALEN, and Cas9. *Mol. Ther.* **27**, 735–746 (2019).
6. R. A. Feldman *et al.*, mRNA vaccines against H10N8 and H7N9 influenza viruses of pandemic potential are immunogenic and well tolerated in healthy adults in phase 1 randomized clinical trials. *Vaccine* **37**, 3326–3334 (2019).
7. S. John *et al.*, Multi-antigenic human cytomegalovirus mRNA vaccines that elicit potent humoral and cell-mediated immunity. *Vaccine* **36**, 1689–1699 (2018).
8. U. Sahin *et al.*, An RNA vaccine drives immunity in checkpoint-inhibitor-treated melanoma. *Nature* **585**, 107–112 (2020).
9. P. S. Kowalski, A. Rudra, L. Miao, D. G. Anderson, Delivering the messenger: Advances in technologies for therapeutic mRNA delivery. *Mol. Ther.* **27**, 710–728 (2019).
10. K. A. Hajj, K. A. Whitehead, Tools for translation: Non-viral materials for therapeutic mRNA delivery. *Nat. Rev. Mater.* **2**, 17056 (2017).
11. A. Akinc *et al.*, The Onpattro story and the clinical translation of nanomedicines containing nucleic acid-based drugs. *Nat. Nanotechnol.* **14**, 1084–1087 (2019).
12. Q. Cheng *et al.*, Dendrimer-based lipid nanoparticles deliver therapeutic FAH mRNA to normalize liver function and extend survival in a mouse model of hepatorenal tyrosinemia type I. *Adv. Mater.* **30**, e1805308 (2018).
13. F. DeRosa *et al.*, Therapeutic efficacy in a hemophilia B model using a biosynthetic mRNA liver depot system. *Gene Ther.* **23**, 699–707 (2016).
14. X. Zhang *et al.*, Functionalized lipid-like nanoparticles for in vivo mRNA delivery and base editing. *Sci. Adv.* **6**, eabc2315 (2020).
15. J. Liu *et al.*, Fast and efficient CRISPR/Cas9 genome editing in vivo enabled by bioreducible lipid and messenger RNA nanoparticles. *Adv. Mater.* **31**, e1902575 (2019).
16. M. Qiu *et al.*, Lipid nanoparticle-mediated codelivery of Cas9 mRNA and single-guide RNA achieves liver-specific in vivo genome editing of *Angptl3*. *Proc. Natl. Acad. Sci. U.S.A.* **118**, e2020401118 (2021).
17. R. Kedmi *et al.*, A modular platform for targeted RNAi therapeutics. *Nat. Nanotechnol.* **13**, 214–219 (2018).
18. Q. Li *et al.*, Engineering caveolae-targeted lipid nanoparticles to deliver mRNA to the lungs. *ACS Chem. Biol.* **15**, 830–836 (2020).
19. F. C. Lam *et al.*, Enhanced efficacy of combined temozolomide and bromodomain inhibitor therapy for gliomas using targeted nanoparticles. *Nat. Commun.* **9**, 1991 (2018).
20. Q. Cheng *et al.*, Selective organ targeting (SORT) nanoparticles for tissue-specific mRNA delivery and CRISPR-Cas gene editing. *Nat. Nanotechnol.* **15**, 313–320 (2020).
21. S. Tenzer *et al.*, Rapid formation of plasma protein corona critically affects nanoparticle pathophysiology. *Nat. Nanotechnol.* **8**, 772–781 (2013).
22. M. P. Lokugamage, C. D. Sago, Z. Gan, B. R. Krupczak, J. E. Dahlman, Constrained nanoparticles deliver siRNA and sgRNA to T cells in vivo without targeting ligands. *Adv. Mater.* **31**, e1902251 (2019).
23. L. Miao *et al.*, Delivery of mRNA vaccines with heterocyclic lipids increases anti-tumor efficacy by STING-mediated immune cell activation. *Nat. Biotechnol.* **37**, 1174–1185 (2019).
24. X. C. Hou *et al.*, Vitamin lipid nanoparticles enable adoptive macrophage transfer for the treatment of multidrug-resistant bacterial sepsis. *Nat. Nanotechnol.* **15**, 41 (2020).
25. X. Zhao *et al.*, Imidazole-based synthetic lipidoids for in vivo mRNA delivery into primary T lymphocytes. *Angew. Chem. Int. Ed. Engl.* **59**, 20083–20089 (2020).
26. S. Sabnis *et al.*, A novel amino lipid series for mRNA delivery: Improved endosomal escape and sustained pharmacology and safety in non-human primates. *Mol. Ther.* **26**, 1509–1519 (2018).
27. S. Lee *et al.*, A systematic study of unsaturation in lipid nanoparticles leads to improved mRNA transfection in vivo. *Angew. Chem. Int. Ed. Engl.* **60**, 5848–5853 (2021).
28. K. A. Hajj *et al.*, Branched-tail lipid nanoparticles potently deliver mRNA in vivo due to enhanced ionization at endosomal pH. *Small* **15**, e1805097 (2019).
29. M. Wang, S. Sun, K. A. Alberti, Q. Xu, A combinatorial library of unsaturated lipidoids for efficient intracellular gene delivery. *ACS Synth. Biol.* **1**, 403–407 (2012).
30. A. Huertas *et al.*, Pulmonary vascular endothelium: The orchestra conductor in respiratory diseases: Highlights from basic research to therapy. *Eur. Respir. J.* **51**, 13 (2018).
31. D. Adam *et al.*, Cystic fibrosis airway epithelium remodelling: Involvement of inflammation. *J. Pathol.* **235**, 408–419 (2015).

32. M. J. Holtzman, D. E. Byers, J. Alexander-Brett, X. Wang, The role of airway epithelial cells and innate immune cells in chronic respiratory disease. *Nat. Rev. Immunol.* **14**, 686–698 (2014).
33. K. J. Kauffman *et al.*, Rapid, single-cell analysis and discovery of vectored mRNA transfection in vivo with a loxP-flanked tdTomato reporter mouse. *Mol. Ther. Nucleic Acids* **10**, 55–63 (2018).
34. R. Cai, C. Chen, The crown and the scepter: Roles of the protein corona in nanomedicine. *Adv. Mater.* **31**, e1805740 (2019).
35. Z. Zhang *et al.*, Corona-directed nucleic acid delivery into hepatic stellate cells for liver fibrosis therapy. *ACS Nano* **9**, 2405–2419 (2015).
36. Z. Zhang *et al.*, Brain-targeted drug delivery by manipulating protein corona functions. *Nat. Commun.* **10**, 3561 (2019).
37. J. Y. Oh *et al.*, Cloaking nanoparticles with protein corona shield for targeted drug delivery. *Nat. Commun.* **9**, 4548 (2018).
38. J. Koo *et al.*, Evaluation of fibrinogen self-assembly: Role of its αC region. *J. Thromb. Haemost.* **8**, 2727–2735 (2010).
39. J. Koo *et al.*, Control of anti-thrombogenic properties: Surface-induced self-assembly of fibrinogen fibers. *Biomacromolecules* **13**, 1259–1268 (2012).
40. M. P. Monopoli *et al.*, Physical-chemical aspects of protein corona: Relevance to in vitro and in vivo biological impacts of nanoparticles. *J. Am. Chem. Soc.* **133**, 2525–2534 (2011).
41. J. B. Miller *et al.*, Non-viral CRISPR/Cas gene editing in vitro and in vivo enabled by synthetic nanoparticle co-delivery of Cas9 mRNA and sgRNA. *Angew. Chem. Int. Ed. Engl.* **56**, 1059–1063 (2017).
42. R. L. Ball, K. A. Hajj, J. Vizelman, P. Bajaj, K. A. Whitehead, Lipid nanoparticle formulations for enhanced co-delivery of siRNA and mRNA. *Nano Lett.* **18**, 3814–3822 (2018).
43. J. J. Bissler *et al.*, Sirolimus for angiomyolipoma in tuberous sclerosis complex or lymphangioleiomyomatosis. *N. Engl. J. Med.* **358**, 140–151 (2008).
44. H. Hua *et al.*, Targeting mTOR for cancer therapy. *J. Hematol. Oncol.* **12**, 71 (2019).
45. Y. Kida, Efficacy and safety of sirolimus in lymphangioleiomyomatosis. *N. Engl. J. Med.* **365**, 271, author reply 272 (2011).
46. M. Ní Bhaoighill, E. A. Dunlop, Mechanistic target of rapamycin inhibitors: Successes and challenges as cancer therapeutics. *MCancer Drug Resist.* **2**, 1069–1085 (2019).
47. F. X. McCormack *et al.*, National Institutes of Health Rare Lung Diseases Consortium; MILES Trial Group, Efficacy and safety of sirolimus in lymphangioleiomyomatosis. *N. Engl. J. Med.* **364**, 1595–1606 (2011).
48. E. A. Goncharova *et al.*, Prevention of alveolar destruction and airspace enlargement in a mouse model of pulmonary lymphangioleiomyomatosis (LAM). *Sci. Transl. Med.* **4**, 154ra134 (2012).
49. K. Maisel *et al.*, Immune checkpoint ligand PD-L1 is upregulated in pulmonary lymphangioleiomyomatosis. *Am. J. Respir. Cell Mol. Biol.* **59**, 723–732 (2018).
50. F. Ma *et al.*, Neurotransmitter-derived lipidoids (NT-lipidoids) for enhanced brain delivery through intravenous injection. *Sci. Adv.* **6**, eabb4429 (2020).
51. M. Wang *et al.*, Efficient delivery of genome-editing proteins using bioreducible lipid nanoparticles. *Proc. Natl. Acad. Sci. U.S.A.* **113**, 2868–2873 (2016).
52. Y. Li *et al.*, Intracellular delivery and biodistribution study of CRISPR/Cas9 ribonucleoprotein loaded bioreducible lipidoid nanoparticles. *Biomater. Sci.* **7**, 596–606 (2019).